IEEE Access
Multidisciplinary ⋮ Rapid Review ⋮ Open Access Journal

Received September 20, 2020, accepted September 28, 2020, date of publication October 7, 2020, date of current version October 20, 2020.

Digital Object Identifier 10.1109/ACCESS.2020.3029397

Degradation Dynamics Cognition and Prediction of Li-Ion Battery: An Integrated Methodology for Alleviating Range Anxiety

LAIFA TAO[1,2], TONG ZHANG[1,2], JIE HAO[1,2], XIAOLIN WANG[3], CHEN LU[1,2], MINGLIANG SUO[1,2], (Member, IEEE), AND YU DING[4]

[1]School of Reliability and Systems Engineering, Beihang University, Beijing 100191, China
[2]Science and Technology on Reliability and Environmental Engineering Laboratory, Beihang University, Beijing 100191, China
[3]Beijing Institute of Control and Electronic Technology, Beijing 100038, China
[4]School of Aeronautic Science and Engineering, Beihang University, Beijing 100191, China

Corresponding author: Yu Ding (dingyu@buaa.edu.cn)

This work was supported in part by the National Natural Science Foundation of China under Grant 61973011, Grant 61803013, and Grant 61903015; in part by the Fundamental Research Funds for the Central Universities under Grant YWF-20-BJ-J-723; in part by the National Key Laboratory of Science and Technology on Reliability and Environmental Engineering under Grant 6142004180501 and Grant WDZC2019601A304; and in part by the China Postdoctoral Science Foundation under Grant 2019M650438.

ABSTRACT We report an integrated methodology (FMC-XGBoost) that mainly consists of a five-state nonhomogeneous Markov chain model (FMC) and XGBoost model. Unlike those existing methods in which capacity fading processes are assumed to be irreversible, the proposed integrated methodology can combine user-specific driving patterns (UDP) and capacity recovery effects (CRE) to predict battery fading dynamics even with partially available data for an individual battery. The parameters of the constructed FMC model are linked to the known physicochemical and material properties of Li-ion battery fading dynamics, which aims to cognize and predict the primary fading dynamics, and the proposed XGBoost model is to cognizes and predicts the fluctuation dynamics regarding UDP & CRE. To comprehensively verify the capabilities of the proposed integrated methodology, a series of cases and comparisons are conducted and analysed based on partial available fading data by selecting batteries to simulate situations of individual differences and different UDPs & CREs. The averages of MAE, MRE and RMSE are approximately 0.0128, 0.9251%, and 0.0153 respectively even when only 60% of the data are available. All verifications and comparison analyses reveal that the proposed integrated methodology provides an accurate, robust, stable, and general way to cognize and predict battery fading dynamics during usage, and subsequently to alleviate range anxiety for batteries in real applications.

INDEX TERMS FMC-XGBoost, fading dynamics prediction, user-specific driving patterns, capacity recovery effects, Li-ion battery, range anxiety.

I. INTRODUCTION

Electric vehicles (EVs) and plug-in hybrid electric vehicles (PHEVs) are recognized as promising green ways to reduce CO2 emission [1]. These vehicles have attracted much attention by many manufacturers around all over the world. However, range anxiety, as one of the major barriers to the large-scale adoption of (P)HEVs, significantly perplexes the vehicles' users [2]. To alleviate range anxiety among (P)HEV drivers, a series of strategies involving the deployment of extensive charging infrastructure, the development of higher battery capacity, battery swapping technology, etc. have been conducted to support the wide use of PHEVs [3].

The associate editor coordinating the review of this manuscript and approving it for publication was Minho Jo.

Actually, for (P)HEV drivers, the concerns are:

1) If the vehicle has sufficient range to reach its destination, i.e., for a given route or a driving plan, whether the real battery capacity (100% state-of-charge) has the capability of reaching the expected destination.
2) How much the batteries have degraded in contrast to the nominal range over a period?

To these ends, one should predict the real battery capacity under the upcoming individual UDP. Thus, one significant way to alleviate range anxiety is to predict the battery fading dynamics of capacity accurately, which will provide sufficient information about the real driving range of the batteries for users.

Generally, the existing prediction approaches can be sorted into model-based, data-driven, and hybrid approaches.

Typically, electrochemical models, electrical equivalent circuit models, and mathematical models are the kernels of model-based approaches, which are conducted to predict the fading dynamics of battery. However, these models are always complicated [4], and the significant reliance on the features with a typical formulation makes it inappropriate to establish models for each kind of battery. In addition, the key parameters of those models are always difficult to be collected in real applications [5], [6]. Data-driven approaches have been conducted in terms of battery fading dynamics prediction of various fields due to easy implementation, inexpensive cost, and less complexity. Statistical methods, as one kind of data-driven approach, are mainly based on the collected time-to-failure data in which prior knowledge is needed such as short voltage sequence [7], [8].

Most of these existing methods have contributed to battery fading dynamics prediction. However, they are mainly based on sufficient datasets throughout the battery whole life as well as a couple of priors, including short voltage sequence, accurate battery model, etc. In addition, regarding capacity loss, most battery prediction models are subject to irreversible degradation, i.e., the CRE is rarely considered when executing battery fading dynamics prediction. However, as figured out by the authors in Ref. [9], CRE significantly affects the fading dynamics of battery. Two kinds of capacity losses, i.e., irreversible and reversible, were clarified by the authors in Ref. [10].

In addition, in (P)HEV applications, the energy usage of large-scale battery systems is strongly correlated with the users' driving patterns which even differ significantly from one driver to another, i.e., the batteries in (P)HEVs suffer from various alternate patterns of 'working-standing'. Take a common route between someone's house and his or her office as an example, and set the house as the start point of a route cycle (one typical user-specific pattern). One should experience ''house (standing) - driving (working) - office (standing) - driving (working)-house (standing)-charging (working) - standing'', where different reversible CRE will take place related to individual pattern.

Thus, it makes sense to integrate UDP & CRE even with only fading and truncated data to give the drivers accurate battery capacity to further alleviate range anxiety.

The standing time slot (STS) and stop-SOC (State of Charge) are main factors that significantly affect CRE [11]. In addition, generally, an arbitrary UDP can be equivalent to a combination of various working states with different stop-SOCs, and different STSs which divide the UDP into various workings. So, to model and predict the fading dynamics of a battery with consideration of UDP & CRE, abstractly, it requires us to combine three factors STS and stop-SOC together for accurate prediction results. In this article, we focus on investigating the two factors to facilitate a unified modelling analysis, and together, apply them to predict battery fading dynamics with only partial and truncated data.

As mentioned in Ref. [12], like analytical models, stochastic models are used to depict batteries theoretically with less time consumption than electrochemical models and better accuracy than the other models. In practice, complex electrochemical reactions taking place within batteries are significantly affected by the factors aforementioned [13]. Compared to other existing models, stochastic models, particularly Markov chain processes [14], can be used to characterize the stochastic nature within batteries.

Among the machine learning methods used in prediction, gradient tree boosting is one technique that shines in many applications. XGBoost is an improvement of machine learning system for tree boosting, which not only can ensure the accuracy and robustness, but can enhance the operation efficiency greatly.

Faced with the aforementioned issues, and with the purpose of maximizing the available partial data, in this study, we set the procedures of capacity fading dynamics cognition and prediction into two main modules. The first one is to cognize the primary fading dynamics, mainly by the proposed five-state nonhomogeneous Markov chain model (FMC) with the inspiration of the four state Markov chain in cognizing the fading dynamics of Li/S batteries [10]. The parameters of FMC are linked to the known physicochemical degradation dynamics and material properties of Li-ion batteries. In addition, the changes in the battery continuous fading process are also modelled by introducing the dynamic transition probability matrix among different cycles, which will further enhance the capability of the FMC model. Further, UDP & CRE modelling is conducted, which will be applied to cognize and predict the fluctuation dynamics based on the XGBoost model which refers to the effects of STS and stop-SOC on Li-ion battery fading dynamics. The fading dynamics for each individual battery with different UDP & CRE can be obtained by adding the primary fading dynamics and fluctuation dynamics correspondingly.

We also conduct a series of experiments by selecting the battery dataset with different individual differences regarding UDP & CRE from NASA to verify the capabilities of the proposed integrated methodology. The qualitative and quantitative analyses conducted in this study suggest that the proposed integrated methodology provides an accurate, robust, stable, and general way to predict battery fading dynamics during usage, and subsequently to alleviate range anxiety.

II. MATERIALS AND METHODS

A. DESCRIPTION OF PROBLEMS

We assume that the whole fading dynamics of Li-ion battery can be decomposed into two parts, i.e., primary fading dynamics and fluctuation dynamics, as a constraint of this problem. Primary fading dynamics are the main part which are related to the state transition of ions inside the battery, and the proposed FMC model could handle this part well. The fluctuation dynamics mainly caused by CRE, which will be determined by STS and stop-SOC, two important

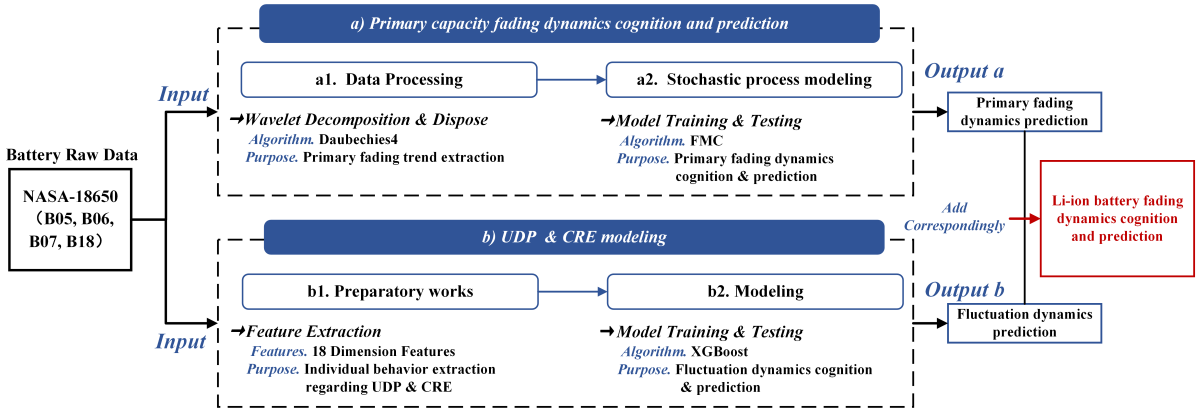

FIGURE 1. The procedure of the proposed FMC-XGBoost methodology.

components of UDP. Therefore, the core problem is how can we establish a mapping between STS and stop-SOC and the capacity fluctuation of battery. Herein, we develop a technology for excavating features regarding STS and stop-SOC, and associate with the XGBoost model to solve this problem.

To simplify the process, we build a qualitative mathematical formula.

$$\begin{aligned} C_W &= C_{primary} + C_{fluctuation} \\ &= f_{FMC}(C_{primary}) + f(CRE, UDP) \\ &= f_{FMC}(C_{primary}) + f_{XGBoost} \\ &\quad \times (STS, stop - Soc, capacity\ fluctuation) \end{aligned} \quad (1)$$

B. TECHNOLOGY STRATEGY

To solve the mentioned problem above step by step, we set two main modules in our methodology. More details can be seen in Fig. 1.

1) PRIMARY CAPACITY FADING DYNAMICS COGNITION AND PREDICTION

a: DATA PROCESSING

We extract the primary trend information of the training data and use it as the input to build the FMC model. After wavelet decomposing, the approximation signals covering the low frequency information and the detailed signals covering the high frequency information are obtained, and the former is the ingredient we need.

b: STOCHASTIC PROCESS MODELLING

For each individual battery, we construct the FMC model based on the primary fading trend acquired in ***a1***. We calculate all six parameters in the model for cognition and prediction, and then, we can obtain the prediction result of primary fading dynamics as the output of this module.

2) UDP & CRE MODELING

a: PREPARATORY WORKS

After analysing the characteristics of the degradation processes, we extract a series of 16 time-related features as well as two other features from training data which are as the inputs of XGBoost model for training and testing.

b: MODELLING

Inspired by the advantages of the XGBoost model, the achieved extracted 18-D features and dc are collected to train and test the XGBoost to model UDP & CRE.

The cognition and prediction of Li-ion battery fading dynamics via FMC-XGBoost with consideration of UDP & CRE can be obtained by adding the outputs of a and b correspondingly. More details of the proposed methodology can be seen in Sections IV-A and IV-B.

C. BATTERY PRIMARY FADING DYNAMICS COGNITION AND PREDICTION

The main fading factor of Li-ion battery on the negative electrode is the development of the solid electrolyte interphase (SEI) [15] over time, which induces an electrolyte decomposition accompanied by a continuous loss of Li-ions [16]. In this article, to cognize and predict the primary fading dynamics within the Li-ion battery, we develop herein the FMC model for battery primary fading process cognition and prediction, which undergoes transitions from one state to another on the battery health state space.

Generally, the five states of FMC can be described as a sequence of random health state variables X_1, X_2, X_3, X_4, X_5 with the Markov property, namely the probability of moving to the next health state depends only on the present health state and not on the previous health states. As a sequence, the health state space of the FMC model is S_1, S_2, S_3, S_4, S_5.

When we employ the FMC model to describe the discharge capacity fading of Li-ion battery, to intuitively describe the FMC model, three phases named hibernating phase, active phase, and absorbing phase, are mentioned, where the five health states are contained, as shown in Fig. 2. The inactive behaviours of the active ionic materials (Li, alloys and others) can be generally depicted by health state S_1 in the hibernating phase, as shown in Fig.2, i.e., the fraction of active materials within this phase does not participate in the regular charge and discharge process, but can be converted into the active phase by chemical reaction within the battery during cycling. In the FMC model, the health state S_1 is assumed to be able to be converted into active health state S_3 (a state of active phase) only, with a conditional transition probability $P(S_3|S_1)$.

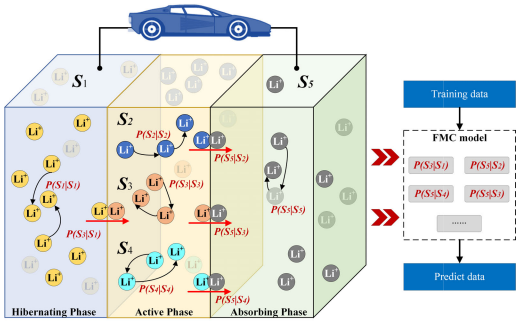

FIGURE 2. The proposed FMC model.

During the early cycling periods, the electrode passivation and/or the film formation of the SEI layer could lead to the decay of electrochemical capacity. S_2 is an active state representing the necessary amount of the active phase for the initial film/slayer formation. $P(S_5|S_2)$ is also a condition transition probability.

The electrode's impedance may lead to the loss of active surface at the SEI when the battery is used for a period. Therefore, the role of the active state S_3 accounts for the phenomena. The materials inside the battery in state S_4 represents their quite stable activity when participating in the long-term charge / discharge process. All the three states, S_2, S_3, and S_4, comprise the second part: the active phase.

The active phase plays an important role in the electrochemical capacity of a Li-ion battery. The quantity of the active materials in the active phrase is equal to the maximum available discharge capacity in some way. The active phase can be deemed as the fraction of Li-ions and/or other active materials that participate in the whole process. Therefore, the measurable maximum available discharge capacity of a Li-ion battery is the sum of the values S_2, S_3 and S_4.

In the absorbing phase, all active substances will be degraded or fixed in other chemical compounds. This phase is denoted by the absorbing state S_5, where the materials cannot contribute to the charging and discharging processes anymore. The transitions among these five states are governed by nine conditional transition probabilities, as shown in Fig. 2.

In Fig. 2 and, generally in this study, a one-step transition from time slot k to time slot $k+1$ represents a one-time use or a charge and discharge cycle (a time slot) of the battery, where Li^+ is employed to denote all active materials for simplicity. The transition probabilities of going from one health state at time slot k to other health states at time slot $k+1$, i.e., $P(X_{k+1} = S_j | X_k = S_i)$ $(i, j \in 1, 2, 3, 4, 5)$ are located near the corresponding arrows in Fig. 2, which together constitute the transition matrix of a time-nonhomogeneous Markov chain.

For simplicity, at time k, $P^{(k)}(S_j|S_i)$ is employed to denote $P^{(k+1)}(X_{k+1} = S_j|X_k = S_i)$.

The state of a fading battery at the math cycle can be represented by a state vector with five fractions:

$$S^{(m)} = \begin{bmatrix} S_1^{(m)} & S_2^{(m)} & S_3^{(m)} & S_4^{(m)} & S_5^{(m)} \end{bmatrix}^T, \quad m = 0, 1, 2, \cdots \tag{2}$$

For arbitrary cycle k, each state S_i is transformed into state S_j with a transition probability $P^{(k)}(S_j|S_i) \times P^{(k)}(S_j)$, where $P^{(k)}(S_j|S_i)P^{(k)}(S_j|S_i)$ is the conditional transition probability. The conditional transition probability is determined by the probability of the active materials shift from state S_iS_i to S_jS_j given that they are originally in state S_iS_i. And $P^{(k)}(S_j)P^{(k)}(S_i)$ is the probability of finding active materials in state S_iS_i. All these probabilities can be written as follow:

$$\begin{aligned} P^{(k)}\left(S_j|S_i\right) &= P\left(X_k = S_j|X_{k-1} = S_i\right) \\ S_{sum}^{(k)} &= S_1^{(k)} + S_2^{(k)} + S_3^{(k)} + S_4^{(k)} + S_5^{(k)} \\ P^{(k)}\left(S_i\right) &= S_i^{(k)} \Big/ S_{sum}^{(k)} i, \quad j \in \{1, 2, 3, 4, 5\} \end{aligned} \tag{3}$$

Thus, for arbitrary cycle kk, the battery fading dynamics of a Li-ion battery can be denoted by a 5×5 transition matrix $T^{(k)}$, (4), as shown at the bottom of the page.

The state vector at cycle (k-1), can be derived by applying $T^{(k)}T^{(k)}$:

$$S^{(k)} = S^{(k-1)}T^{(k)} \tag{5}$$

For a given initial state, $S^{(0)}$, of a Li-ion battery, the state vector of a battery at the k^{th} time slot is:

$$S^{(k)} = \prod_k [S^{(0)} \cdot T^{(k)}] \tag{6}$$

In a certain given aging status of the battery, the transition ability among each state is different; here, in the proposed FMC model, the transition probabilities are set to change over time. Exponential functions are utilized to express the transition probability matrix. For simplicity, only $P^{(k)}(S_5|S_4)$ is set to change over time since the stable active state determines the primary trend. Each transition probability of a fading battery at a cycle when $k \geq 2$ is written as:

$$\begin{aligned} P^{(k)}\left(S_5|S_4\right) &= \begin{cases} \dfrac{e^{\frac{\theta_{45}}{k}} - e^{\frac{\theta_{45}}{k-1}}}{1 - e^{\frac{\theta_{45}}{k-1}}} & k \geq 2 \\ 1 - e^{\theta_{45}} & k = 1 \end{cases} \\ P^{(k)}\left(S_5|S_2\right) &= 1 - e^{\theta_{25}} \\ P^{(k)}\left(S_3|S_1\right) &= 1 - e^{\theta_{13}} \end{aligned} \tag{7}$$

$$T^{(k)} = \begin{Vmatrix} 1 - P^{(k)}(S_3|S_1) & 0 & 0 & 0 & 0 \\ 0 & 1 - P^{(k)}(S_5|S_2) & 0 & 0 & 0 \\ P^{(k)}(S_3|S_1) & 0 & 1 - P^{(k)}(S_5|S_3) & 0 & 0 \\ 0 & 0 & 0 & 1 - P^{(k)}(S_5|S_4) & 0 \\ 0 & P^{(k)}(S_5|S_2) & P^{(k)}(S_5|S_3) & P^{(k)}(S_5|S_4) & 1 \end{Vmatrix} \tag{4}$$

where θ_{13}, θ_{25}, θ_{45} are the three dimensionless parameters required to be estimated.

Since the number of Li-ions in S_3 is quite less than those in S_4, in the interest of simplicity, $P^{(k)}(S_5|S_3)$ and $S_3^{(1)}$ are assumed to be 0. Thus, the simplified transition matrix at time slot k should be rewritten in (8), as shown at the bottom of the page.

As aforementioned, the sum of all active states represents the maximum available discharge capacity of a battery. Thus, the maximum discharge capacity can be written as:

$$C^{(k)} = S_2^{(k)} + S_3^{(k)} + S_4^{(k)} \tag{9}$$

By applying (6) and (8) to (9), we can obtain:

$$\begin{aligned} C^{(k)} &= S_2^{(k)} + S_3^{(k)} + S_4^{(k)} \\ &= \left\{S_2^{(k-1)} \times \left[1 - P^{(k)}\left(S_5|\, S_2\right)\right]\right\} \\ &\quad + \left\{S_1^{(k-1)} \times P^{(k)}\left(S_3|\, S_1\right) + S_3^{(k-1)}\right\} \\ &\quad + S_4^{(k-1)} \times \left[1 - P^{k}\left(S_5|\, S_4\right)\right] \end{aligned} \tag{10}$$

Thus, by combining (7), it yields:

$$\begin{aligned} C^{(k)} &= S_2^{(k)} + S_3^{(k)} + S_4^{(k)} \\ &= \left\{S_2^{(k-2)} \times e^{\theta_{25}\times 2}\right\} + \left\{S_1^{(k-2)} \times \left(1 - e^{\theta_{13}\times 2}\right) + S_3^{(k-2)}\right\} \\ &\quad + S_4^{(k-1)} \times \left[\frac{1 - e^{\frac{\theta_{45}}{k}}}{1 - e^{\frac{\theta_{45}}{k-1}}}\right] \times \left[\frac{1 - e^{\frac{\theta_{45}}{k-1}}}{1 - e^{\frac{\theta_{45}}{k-2}}}\right] \\ &= S_1^{(0)} \times \left(1 - e^{\theta_{13}\times k}\right) + S_2^{(0)} \times e^{\theta_{25}\times k} \\ &\quad + S_4^{(0)} \times \left(1 - e^{\frac{\theta_{45}}{k}}\right) \end{aligned} \tag{11}$$

with three linear constraints:

$$\begin{aligned} \theta_{13} &< 0 \\ \theta_{25} &< 0 \\ \theta_{45} &< 0 \end{aligned} \tag{12}$$

D. UDP & CRE MODELLING

As aforementioned, in this article, STS and stop-SOC have been considered to investigate UDP & CRE. Herein, we find a way to model these two elements by employing XGBoost. In this study, STS has been represented by a series of standing-time-related features (refer to Section IV-B(1)), based on which the detailed relationship between UDP & CRE and STS & stop-SOC will be modelled with the help of XGBoost.

For the Gradient Boosting Decision Tree (GBDT) algorithm, only the derivative information of the first order can be used. When training the nth tree, it is necessary to employ the residual error of the former $(n-1)$ tree, which makes it difficult to achieve the expected distributions. To find the optimal solution, the loss function of XGBoost is expressed by using a 2 order Taylor expansion joined with corresponding regularization process. Therefore, there is a trade-off between the decline of the loss function and the complexity of the model to avoid fitting.

With the improvement of prediction accuracy, another highlight of XGBoost is that it can automatically use the multi-threading of CPU to perform parallel operations, which takes less time than GBDT. The efficient operation speed of XGBoost can be applied to various engineering fields, including diagnosis, prognostics, etc.

For prediction by XGBoost, the raw dataset should be firstly divided into multiple sub-datasets, and then each sub-dataset would be randomly assigned to a base classifier for prediction. The final prediction results of XGBoost are calculated based on all predicted results as well as the predetermined weights of all base classifiers.

The steps of the algorithm are as follows:

1) The objective function of the algorithm is:

$$L = \sum_i l(\hat{y}_i, y_i) + \sum_k \Omega(f_k) \tag{13}$$

where we assume the model has K decision trees

$$\hat{y}_i = \sum_{k=1}^{K} f_k\left(x_i\right) \tag{14}$$

Decision tree complexity function:

$$\Omega(f) = \gamma T + \frac{1}{2}\lambda \|w\|^2 \tag{15}$$

where T is the number of leaves, w is the weight of the leaves, and$\hat{y}_i^{(t)} = \hat{y}_i^{(t-1)} + f_t\left(x_i\right)$.

2) Training objective function:

$$L^{(t)} = \sum_{i=1}^{n} l\left(\hat{y}_i^{(t-1)} + f_t\left(x_i\right), y_i\right) + \Omega\left(f_t\right) \tag{16}$$

3) Taylor's quadratic approximation of the target function: Second-order approximation can be used to quickly optimize the objective in the general setting.

$$L^{(t)} \cong \sum_{i=1}^{n} [l\left(y_i, \hat{y}_i^{(t-1)}\right) + g_i f_t(x_i) + \frac{1}{2} h_i f_i^2(x_i)] + \Omega(f_t) \tag{17}$$

$$T^{(k)} = \begin{Vmatrix} 1 - P^{(k)}\left(S_3|S_1\right) & 0 & 0 & 0 & 0 \\ 0 & 1 - P^{(k)}\left(S_5|S_2\right) & 0 & 0 & 0 \\ P^{(k)}\left(S_3|S_1\right) & 0 & 1 & 0 & 0 \\ 0 & 0 & 0 & 1 - P^{(k)}\left(S_5|S_4\right) & 0 \\ 0 & P^{(k)}\left(S_5|S_2\right) & 0 & P^{(k)}\left(S_5|S_4\right) & 1 \end{Vmatrix} \tag{8}$$

where $g_i = \delta^2_{\hat{y}(t-1)} l(y_i, \hat{y}^{(t-1)})$ is the first derivative of the sample and $h_i = \delta^2_{\hat{y}(t-1)} l(y_i, \hat{y}^{(t-1)})$ is the second derivative of the sample.

4) Remove the constant terms to obtain the following simplified objective at step t.

$$\bar{L}^{(t)} = \sum_{i=1}^{n} \left[g_i f_i(x_i) + \frac{1}{2} h_i f_t^2(x_i) \right] + \Omega(f_t) \tag{18}$$

5) Find the optimal solution of the objective function. Define $I_j = \{i|q(x_i) = j\}$ as the j^{th} leaf spot. We can obtain:

$$\begin{aligned} \bar{L}^{(t)} &= \sum_{i=1}^{n} \left[g_i f_t(x_i) + \frac{1}{2} h_i f_t^2(x_i) \right] + \gamma T + \frac{1}{2}\lambda \|w\|^2 \\ &= \sum_{i=1}^{n} \left[g_i f_t(x_i) + \frac{1}{2} h_i f_t^2(x_i) \right] + \gamma T + \frac{1}{2}\lambda \sum_{j=1}^{T} w_j^2 \\ &= \sum_{j=1}^{T} \left[\left(\sum_{i \in I_j} g_i \right) w_j + \frac{1}{2} \left(\sum_{i \in I_j} h_i + \lambda \right) w_j^2 \right] + \gamma T \end{aligned} \tag{19}$$

Then we take the derivative of the top equation and make the derivative result equal to 0. Then,

$$w_j^* = -\frac{\sum_{i \in I_j} g_i}{\sum_{i \in I_j} h_i + \lambda} \tag{20}$$

We can substitute the optimal solution w_j^* for w_j into the target function. We can obtain the optimal solution of the objective function:

$$\bar{L}^{(t)}(q) = -\frac{1}{2} \sum_{j=1}^{T} \frac{\left(\sum_{i \in g_i} g_i \right)^2}{\sum_{i \in I_i} h_i + \lambda} + \gamma T \tag{21}$$

XGBoost uses a greedy algorithm that adds segmentation to existing leaf nodes. Suppose I_L and I_R are the sets of left and right nodes, the information gain is as follows,

$$Gain = \frac{1}{2} \left[\frac{\left(\sum_{i \in I_L} g_i \right)^2}{\sum_{i \in I_L} h_i + \lambda} + \frac{\left(\sum_{i \in I_R} g_i \right)^2}{\sum_{i \in I_R} h_i + \lambda} - \frac{\left(\sum_{i \in I} g_i \right)^2}{\sum_{i \in I} h_i + \lambda} \right] - \gamma \tag{22}$$

III. DATASET DESCRIPTION AND MODEL VERIFICATION OUTLINE

A. BRIEF DESCRIPTION OF THE NASA LI-ION BATTERY DATASET

In this study, a series of cases are investigated based on the entire capacity fading datasets collected from a custom-built battery set up at the NASA Ames Prognostics Center of Excellence to verify the efficiency of the proposed FMC-XGBoost methodology.

The custom-built experimental setup primarily consisted of a set of Li-ion cells (rechargeable 18650-size Gen 2 Li-ion cells with the same rated capacity of 2 Ah), chargers, loads, electrochemical impedance spectrometry equipment, a suite of sensors (voltage, current, and temperature), some custom switching circuitry, a data acquisition system, and a computer for control and analysis [17]. The experiments can be abstracted through four different operational profiles (charging, discharging, impedance measuring, and standing). The charge runs were in constant current (CC) mode at 1.5 A until the battery voltage reached 4.2 V and continued in constant voltage mode until the charge current dropped to 20 mA. Discharging was conducted and stopped at different end-of discharges (EODs). Impedance measurement was performed during the charging and discharging processes. Standing took place whenever a battery did not experience any of the former three profiles. The experiments were conducted until the capacity decreased to the specified end-of-life criteria (EOLC).

TABLE 1. Typical data for testing the efficiency of the proposed model.

ID	CC(A)	DC(A)	EODs(V)	EOLC
B05	1.5	2	2.7	30%
B06	1.5	2	2.5	30%
B07	1.5	2	2.2	30%
B18	1.5	2	2.5	30%

Generally, since all standing profiles are irregularly distributed throughout the experiments, one can refer to the raw data for details.

Different stop-SoCs can be represented by different EODs, and the STSs can be divided into a series of features regarding standing time (related to UDP & CRE). One can see the details of the extracted features of STS in Section IV-B(1). Furthermore, the situations of partial available of fading data will be simulated based on the selected typical data (B05, B06, B07, and B18) shown in Table 1.

B. VERIFICATION OUTLINE

A series of cases have been designed and investigated. Two prediction cases and 3 contrast cases are introduced as follows.

Case 1 (Section IV-A). The FMC model is employed to cognize and predict the primary fading dynamics even when only partial fading data is available.

Case 2 (Section IV-B). In this case, the proposed FMC-XGBoost methodology is an integrated method which combines the FMC model with the XGBoost model.

Based on the prediction cases, we further set a series of contrasting cases, which are Case 4, 5, and 6.

Case 3 (Section V-A). FMC vs. FMC-XGBoost. We compare the prediction results of the proposed stochastic model FMC and the proposed integrated model FMC-XGBoost. In this section, one can see that great improvements in predicting and dynamic tracking have been achieved by considering UDP & CRE based on the proposed integrated model FMC-XGBoost.

Case 4 (Section V-B). FMC-XGBoost predict in various amount of training data available. To mimic real-life usage scenarios as much as possible and to test the adaptability and robustness of FMC- XGBoost which is critical for real

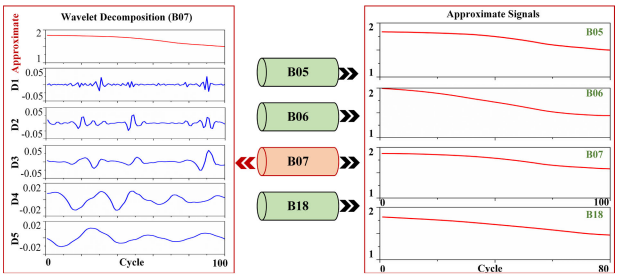

FIGURE 3. Approximate signals of all batteries and all components of B07.

applications, four typical and different amounts of training data are used.

Case 5 (Section V-C). FMC-XGBoost vs. reported typical models. We examine a series of typical approaches which have been proven to be effective in cognizing nonlinear dynamics especially for Li-ion battery prediction, to verify the effectiveness of our proposed methodology with the same metrics for an intuitive and direct comparison.

We employ 60% of the entire data of each battery to train and cognize battery fading dynamic, and then predict the following fading dynamics, i.e., the former 100 cycles of datasets of B05, B06, and B07 are utilized for feature extraction and training, while only the former 80 cycles are employed for B18. The rest of the cycles of each battery dataset will be used to test the proposed FMC-XGBoost methodology.

IV. EXPERIMENTAL EVALUATIONS

A. PREDICTION WITHOUT CONSIDERATION OF UDP &CRE: THE PROPOSED STOCHASTIC MODEL (FMC)

1) PRIMARY FADING DYNAMICS COGNITION BASED ON PARTIAL FADING DATA

By referring to [18], Daubechies4(db4) is selected accompanied with decomposition layers of 5. Fig. 3 shows the corresponding approximate signals of all batteries and all components of B07 as an example of wavelet decomposition.

In Fig. 3, the approximate signals, which demonstrate and contain the primary fading trend of the partial fading data of each battery, are the expected primary fading dynamics and will be used further to establish the proposed FMC model. Moreover, the approximate signals differ from each other, which can be regarded as one aspect of individual differences.

The proposed FMC is a five-state nonhomogeneous Markov chain model, which generally has a parameter vector of six unknown parameters (see (11)), i.e., to establish the FMC model for each battery. Different parameter vectors come with different fading dynamics and vice versa. The purpose we develop FMC model is to cognize the primary fading dynamics within each partial fading data, and then predict with each established FMC model with the estimated parameter vector.

Herein, the FMC model is trained by using the decomposition approximate signals of partial fading data of each battery and then is utilized to cognize the primary fading dynamics of the rest of the fading data of the corresponding battery.

TABLE 2. Estimated parameters of the FMC model of B07 when 60% of the data are available.

Parameters	$S_1^{(1)}$	$S_2^{(1)}$	$S_4^{(1)}$	θ_{13}	θ_{25}	θ_{45}
B07	1.1537	0.3797	1.5113	-0.0037	-0.0171	-140.3326

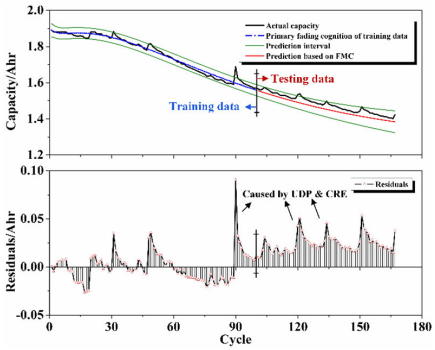

FIGURE 4. The predicted primary fading dynamics based on FMC (B07).

TABLE 3. Quantitative analysis on the primary fading dynamics and prediction (FMC model).

Metrics	MAE	MRE/%	RMSE
B07	0.0240	1.6237	0.0259

As shown in Table 2, the corresponding parameters of the FMC model for B07 battery are estimated for example.

Once those parameters which reflect the primary fading dynamics of each battery are achieved, the corresponding established FMC can be used to make predictions.

2) PREDICTION BASED ON FADING DYNAMICS COGNITION

For different batteries, the start points of prediction are the first ones following the last points of available fading data, i.e., 101st for B05, B06, B07, and 81st for B18. Fig. 4 intuitively demonstrates the prediction result of the primary fading dynamics as well as the corresponding residuals of B07.

As seen from the residuals in Fig. 4, there are several obvious fluctuations in both the training and testing parts. These fluctuations caused by UDP & CRE cannot be cognized and predicted by FMC which will inevitably enlarge the errors of fading dynamics prediction, accompanying with uncertainties.

In this study, a series of uncertain deviations of capacity may take place during the battery fading process due to the integrated effects of UDP & CRE. To this end, in Section IV-B, the FMC-XGBoost methodology is proposed to figure out those effects introduced by UDP & CRE, which will enhance the accuracy and stability of fading dynamics prediction.

B. FADING DYNAMICS COGNITION & PREDICTION WITH CONSIDERATION OF UDP & CRE: THE PROPOSED FMC-XGBOOST METHODOLOGY

1) INPUTS CONSTRUCTION FOR UDP & CRE MODELLING

Herein, 16 standing-time-related features are extracted to recognize the relationship between UDP & CRE and STS.

For clear understanding, herein, all these 16 features (standing time interval, STI) are introduced accompanied with succinct notations and descriptions.

D2D: The STI between the start points of every two continuous discharging processes; ***D2C***: The STI of the start points of the discharging process and the following charging process; ***D2E***: The STI of the start points of the discharging process and the following impedance measurement. ***C2C***, ***C2D***, ***C2E***, ***E2E***, ***E2C***, ***E2D*** are defined in the same way, in which, '***C***' represents 'charging processes' and '***E***' represents 'impedance measurement'. ***M-C2D***: The difference between two continuous '***C2D***', and in the same way, ***M-D2C***, ***M-E2C***, ***M-C2E***, and ***M-D2E*** are defined. ***Dist***: The distance between the current start point of a discharging process and that of another discharging process which is in the neighbourhood of the current discharging process that lasts the longest.

In addition to the 16 standing-time-related features, stop-SoC (denoted SS in Feature) and cycling number (CN) are treated as the other two features, which is adopted to reflect UDP & CRE. Hereto, all factors regarding UDP & CRE are considered and can be summarized and extracted from real applications for training and predicting, such as the given routes and driving plan. For each feature of STS and stop-SoC, the extracted values vary over CN, which illustrates and simulates one kind of UDP & CRE in application, i.e., it makes sense for us to combine all these UDP & CRE extracted from all the selected batteries together to simulate the cases in real applications.

2) OUTPUTS CONSTRUCTION FOR UDP & CRE MODELLING

Once the features regarding UDP & CRE are obtained, we need to find out the fluctuation dynamics regarding UDP & CRE for each battery, which will be treat as the outputs (dependent variable) of the XGboost model.

To construct the outputs, the first thing is to calculate the residuals between the measured capacities and the estimated and predicted capacities by the established FMC models with the estimated parameters (refer to Section IV-A). Then, the difference values (denoted ***dc***) of the continuous residuals for each battery are calculated by (23):

$$dc(i) = r(i+1) - r(i) \tag{23}$$

dc is a parameter that represents the fluctuation of capacity mostly caused by UDP & CRE. To simplify the model, we ignore the random noises and regard ***dc*** as the dependent variable of the XGBoost model. Once the XGBoost model is trained, the predicted ***dc*** will be obtained with the features mentioned in Section IV-B(1) which can be counted and calculated in the real applications.

Same as the data structure used in Section IV-A, the former 60% partial dc of all selected batteries and the features regarding UDP & CRE will be used as the dependent variable to train the XGBoost model. The rest 40% of the data of each battery will be employed to evaluate the effectiveness of the established FMC-XGBoost model on battery fading dynamics cognition and prediction.

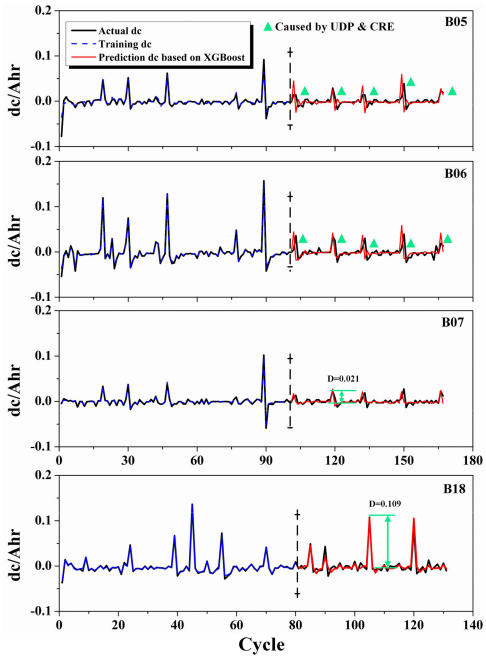

FIGURE 5. The predicted dc of the rest of the 40% data of each battery.

3) PREDICTION BASED ON THE PROPOSED FMC-XGBOOST METHODOLOGY

The blue and red lines in Fig. 5 demonstrate the cognized and predicted ***dc*** under a specific UDP & CRE, respectively. As we can see intuitively, in all cases, most of the predicted ***dc*** values are consistent with the real ***dc*** values calculated. Especially, the inhomogeneously distributed extreme points which present different location characteristics from battery to battery in Fig. 5 can be understood as the outcomes of UDP & CRE.

The predicted red lines follow the real actual ***dc*** values well in all batteries which demonstrates the powerful ability of the proposed XGBoost model in handling different UDP & CRE. Importantly, from Fig 5, one can see a minor ***dc*** value (0.021) of B07 and a significantly bigger dc value (0.109) of B18. Faced with huge differences, the predicted ***dc*** stays the same as the actual ***dc***, which indicate the high adaptability and accuracy of the information mining of UDP & CRE.

The favourable results obtained in this step can lay a foundation for the accurate prediction of the results in the next step.

Once the predicted values of ***dc*** are obtained, the fluctuation dynamics regarding UDP & CRE of each battery can be calculated, respectively. To further achieve the final expected predictions of the rest of the 40% data of each battery, the predicted primary fading dynamics and the predicted fluctuation dynamics regarding UDP & CRE of each battery should be added up correspondingly, i.e., the final expected predictions of each battery are the sum of the predictions of the primary fading dynamics (the outputs of the FMC model) and the corresponding predicted fluctuation dynamics regarding UDP & CRE obtained by the XGBoost model, as shown by the red lines in Fig. 6.

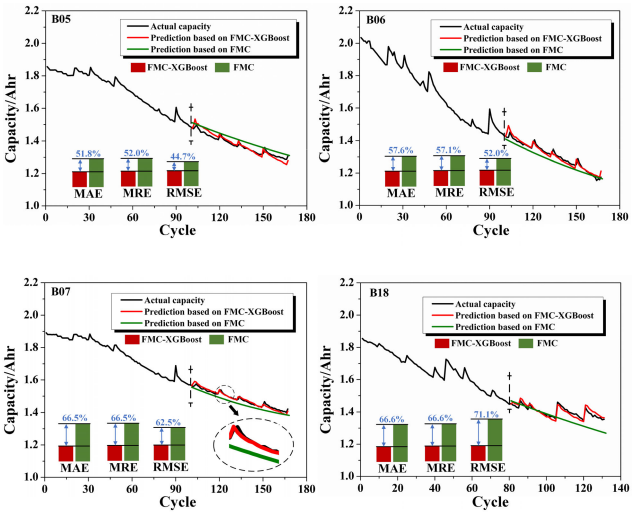

FIGURE 6. Fading dynamics cognition & prediction (FMC-XGBoost).

Intuitively, the predicted signal based on FMC-XGBoost and the actual capacity basically coincide with each other. For a detailed data display, all metrics of each battery are labelled in Fig. 6. The MAE ranges from 0.0081 to 0.0144, the MRE% ranges from 0.5541% to 1.0289% and the RMSE ranges from 0.0097 to 0.0169, which stay relatively steady at low levels. All these metrics illustrate that the proposed FMC-XGBoost methodology has high adaptability and stability adapted to different individuals with different UDP & CRE.

V. DISCUSSIONS

A. THE EFFICIENCY ANALYSIS OF PREDICTION WITH CONSIDERATION OF UDP & CRE

Facing individual differences, we compare all prediction performance of the proposed stochastic model FMC and the proposed integrated model FMC-XGBoost by examing the case values of the corresponding metrics in SectionIV-A(2) and IV-B(3). The detailed comparison can be seen in the histograms of Fig. 6 case by case. Illustrated in Fig. 6, the averages of the statistical metrics, MAE, MRE and RMSE are reduced conspicuously by 60.6 %, 60.6 % and 57.6 %, respectively. Moreover, the RMSE which is a popular metric in predictive performance evaluation of FMC-XGBoost reduced by 44.7%, 52.0%, 62.5% and 71.1% respectively. Overall, there are huge improvements for all four batteries. A maximum reduction by 71.1% and the biggest fluctuations can be both seen in B18 from Fig. 10 indicating that the proposed FMC-XGBoost can cognize and predict the primary and fluctuation dynamics well. Meanwhile the partial enlarged drawing in the subgraph of B07 visually shows the precise dynamic tracking capability in battery capacity fading prediction.

The most important factor contributing to these improvements is the UDP & CRE modelling. So, it can be concluded that the proposed FMC-XGBoost methodology is powerful in handling the effects of UDP & CRE and in predicting the fading dynamics.

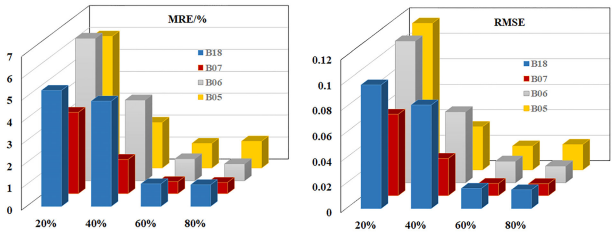

FIGURE 7. Prediction metrics under different partial data availabilities.

B. ADAPTABILITY AND ROBUSTNESS ANALYSIS OF FMC-XGBOOST

In all cases mentioned, 60% of the entire data are employed to train the models and is utilized to cognize and predict the fading dynamics of the rest 40% of the entire data of the corresponding battery. For generally verification, herein, we conduct and train the proposed integrated methodology based on other typical partial cases, say 20%, 40%, and 80% of the entire data, and then to cognize and predict the rest fading dynamics.

For visualization, here, MRE and RMSE are selected for a concise description. As we can see from Fig. 7, the averages of MRE and RMSE are 5.3705% and 0.0969 when 20% data are available, i.e., one can make the prediction of the capacity with an accuracy more than 90% even based on a considerably small amount of data. From the overall point of view, with the increase of data proportion, the prediction accuracies of the models keep improving, which can be seen from Fig. 7. Together, one can see that the proposed methodology has a high capability of 1) learning the driving pattern even with very limited data; 2) cognizing and predicting the fading dynamics throughout a battery lifetime; 3) adapting to the given user-specific patterns and/or driving plans; 4) providing stable and credible information for a driver which is significant for real applications.

C. COMPARATIVE ANALYSIS WITH THE REPORTED TYPICAL MODELS

Several reported typical models which have been proven to be effective in cognizing and predicting battery fading dynamics, are examined in this article [19]–[22]. Herein, some further comparison will be conducted for a comprehensive verification of the effectiveness of the proposed FMC-XGBoost model.

A couple pieces of information on the proposed and the referenced approaches such as model name, predicting mode, and data structure of training and testing, are listed in Table 4. For a deep comparison, those quoted approaches have been divided into three groups (***a***, ***b*** and ***c***) according to differences among the predicting mode, training data, and testing data.

Note that, in this study, the proposed FMC-XGBoost methodology has been applied to all four batteries B05, B06, B07, and B18, which have been widely employed to verify published models. However, for comparison, the same battery and metrics as well as similar data structures are chosen according to the situations within each corresponding group.

TABLE 4. Introductions of the contrast models.

Group	Model	Predicting mode	Training data	Testing data
a	NASA_PF [21]	Extrapolated prediction	0-80 cycles of B18 (former 60% of all available data) (one-time-training)	80-132 cycles (rest 40%)
	ND-AR_RPF [21]		0-60 cycles of B18 (former 60% of all available data) (one-time-training)	60-100 cycles (rest 40%)
b	CNN [22]	Extrapolated prediction	All fading data of 3 batteries among B05, B06, B07, B18 (one-time-training)	All fading data of the rest one battery
	MC-LSTM[22]			
c	SE-MGPR [20]	One-step- iterative prediction	Iterative training and testing	Fading data of the same battery
	BM-PF[19]			
Herein	FMC-XGBoost	Extrapolated prediction	(former 60% of all available data in each battery) (one-time-training)	Rest 40% data of each battery

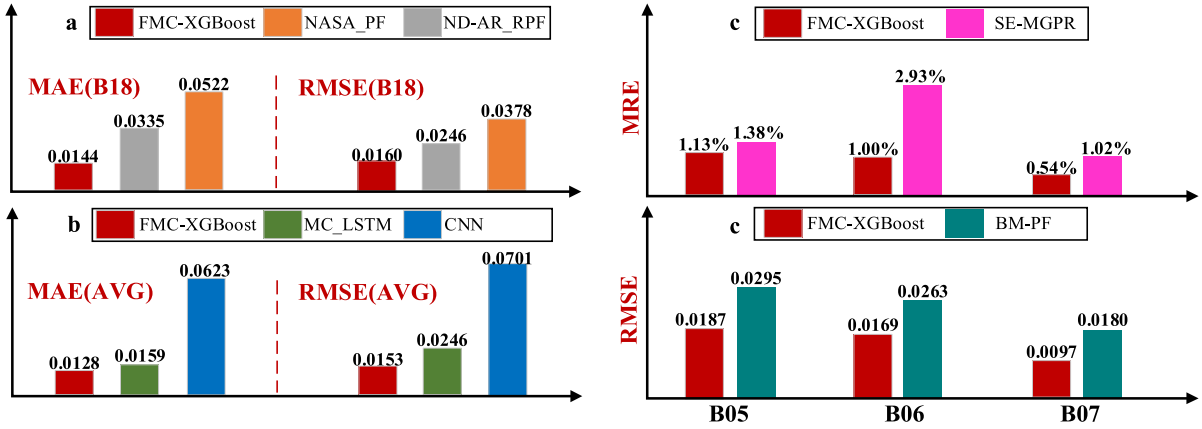

FIGURE 8. Quantitative analysis (reported typical models vs. FMC-XGBoost).

(e.g., the fading dynamics prediction results regarding B18 with the former 60% of fading data for training, accompanied with the metrics of MAE and RMSE, will be employed to verify the efficiency of the proposed methodology by comparing with [21], [22] where only B18 was selected and tested using the metrics of MAE and RMSE.

***Group a*: Model-based approaches, i.e., NASA_PF and ND-AR_RPF**

In this group, the referenced approaches and the proposed one have a similar data structure of the former 60% of data. More importantly, as shown in Fig. 8, the last 32 cycles of B18 demonstrating great fluctuations which always highly increase the difficulty and uncertainty of prediction were not considered in [21]. However, one obvious conclusion that can be achieved is that our integrated methodology is with higher accuracy and

stability according to comparisons via both MAE (reduced by 72.4% and 57.0% respectively) and RMSE (reduced by 57.7% and 35.0% respectively), as shown in Fig. 8(a).

***Group b*: Deep learning approaches, i.e., CNN and LSTM**

In this group, to predict one battery fading dynamics, say B05, all fading data of the other three batteries, say B06, B07, and B18, were used to train the corresponding model, where at least three complete fading dynamics pictures from the very beginning to the end-of-life were available for comprehensive modelling rather than the extreme data situation, i.e., only one individual partial fading dynamics, which has been used in our methodology. As shown in Fig. 8(b), the proposed FMC-XGBoost has a better prediction performance by using only partial fading data of each individual battery.

***Group c*: Hybrid approaches, i.e., SE-MGPR and BM-PF**

In this group, each battery dynamics were modelled and predicted by hybrid approaches, i.e., SE-MGPR and BM-PF. Different from the extrapolated prediction applied in this study, Fig. 8(c) demonstrates all metrics on B05, B06, and B07 for both SE-MGPR and BM-PF by executing a one-step-iterative prediction which always has very high prediction accuracy. However, the proposed methodology gives a series of perfect MREs and RMSEs.

Combining the comparisons, the advantages of our proposed FMC-XGBoost methodology in fading dynamics cognition and prediction are comprehensive verified. Benefit from UDP & CRE modeling, we can obtain the primary dynamics and especially the fluctuation dynamics for each battery even with individual partial fading data.

D. THE ALLEVIATION OF USERS' RANGE ANXIETY

The main concern of this article is users' range anxiety which may happens in everyone' s daily routine. To minimize the users' anxiety, numerous efforts have been made in this article. Faced with individual differences and real applications, we select battery data with different characteristics, consider the partial data condition, conduct UDP & CRE modelling and build the integrated methodology, i.e., FMC-XGBoost. A tremendous improvement in the prediction accuracy has been made by considering UDP & CRE, meanwhile, the robustness, stability, and dynamic tracking capability in prediction have also been verified based on different individual partially available data. Combining all these efforts, the fading dynamics prediction of batteries can be grasped accurately, i.e., the real battery health conditions subject to the driver's specific pattern at different fading stages can be accurately cognized and predicted, which would provide powerful information in the decision making of whether it is suitable to still use the battery or when it is the right time to exchange the battery for a new one (given a lifetime threshold). All these together will inevitably enhance the user experience on (P)HEV as well as alleviate range anxiety.

VI. CONCLUDING REMARKS AND OUTLOOK

To achieve accurate prediction results and alleviate range anxiety in (P)HEV applications, we introduce an integrated methodology combining FMC and XGBoost in which UDP & CRE are considered. To comprehensively verify the proposed integrated methodology as well as to analyse on how to employ the methodology to cognize and predict fading dynamics with partial fading data availability, a series of cases are conducted step by step based on the published NASA dataset, where the situations regarding individual differences of batteries and different UDP & CRE in real applications are simulated by the selected batteries. Typically, the averages of MAE, MRE and RMSE achieved by the proposed methodology are 0.0128, 0.9251% and 0.0153 with consideration of UDP & CRE when only 60% of the entire data are available.

Further qualitative and quantitative comparison analysis conducted in this study suggests that the proposed methodology has a considerable high capability of learning driving patterns even with very limited data, cognizing and predicting fading dynamics throughout a battery lifetime, and providing stable and credible information to a driver which is significant for real applications. All together makes it a promising way to alleviate users' range anxiety. Future researches to be carried out following this study would be: 1) Datasets collected from real applications with individual UDP will be acquired and employed in the study. 2) Other effects, such as temperature will be integrated into the modelling process.

REFERENCES

[1] Y. Xia, J. Yang, F. Wang, and Q. Cheng, "Impact of battery size and energy cost on the market acceptance of blended plug-in hybrid electric vehicles," *Procedia Comput. Sci.*, vol. 131, pp. 377–386, May 2018, doi: 10.1016/j.procs.2018.04.217.

[2] V. R. Tannahill, M. A. Masrur, D. Sutanto, and K. M. Muttaqi, "Future vision for reduction of range anxiety by using an improved state of charge estimation algorithm for electric vehicle batteries implemented with low-cost microcontrollers," *IET Electr. Syst. Transp.*, vol. 5, no. 1, pp. 24–32, Mar. 2015, doi: 10.1049/iet-est.2014.0013.

[3] A. Le Duigou, Y. Guan, and Y. Amalric, "On the competitiveness of electric driving in France: Impact of driving patterns," *Renew. Sustain. Energy Rev.*, vol. 37, pp. 348–359, Sep. 2014, doi: 10.1016/j.rser.2014.04.056.

[4] G. Giordano, V. Klass, M. Behm, G. Lindbergh, and J. Sjoberg, "Model-based lithium-ion battery resistance estimation from electric vehicle operating data," *IEEE Trans. Veh. Technol.*, vol. 67, no. 5, pp. 3720–3728, May 2018, doi: 10.1109/TVT.2018.2796723.

[5] M. S. Haque, S. Choi, and J. Baek, "Auxiliary particle filtering-based estimation of remaining useful life of IGBT," *IEEE Trans. Ind. Electron.*, vol. 65, no. 3, pp. 2693–2703, Mar. 2018, doi: 10.1109/TIE.2017.2740856.

[6] Z. Liu, G. Sun, S. Bu, J. Han, X. Tang, and M. Pecht, "Particle learning framework for estimating the remaining useful life of lithium-ion batteries," *IEEE Trans. Instrum. Meas.*, vol. 66, no. 2, pp. 280–293, Feb. 2017, doi: 10.1109/TIM.2016.2622838.

[7] X. Hu, J. Jiang, D. Cao, and B. Egardt, "Battery health prognosis for electric vehicles using sample entropy and sparse Bayesian predictive modeling," *IEEE Trans. Ind. Electron.*, vol. 63, no. 4, pp. 2645–2656, Apr. 2016, doi: 10.1109/TIE.2015.2461523.

[8] R. Kontar, J. Son, S. Zhou, C. Sankavaram, Y. Zhang, and X. Du, "Remaining useful life prediction based on the mixed effects model with mixture prior distribution," *IISE Trans.*, vol. 49, no. 7, pp. 682–697, Jul. 2017, doi: 10.1080/24725854.2016.1263771.

[9] L. Tao, J. Ma, Y. Cheng, A. Noktehdan, J. Chong, and C. Lu, "A review of stochastic battery models and health management," *Renew. Sustain. Energy Rev.*, vol. 80, pp. 716–732, Dec. 2017, doi: 10.1016/j.rser.2017.05.127.

[10] S. Risse, S. Angioletti-Uberti, J. Dzubiella, and M. Ballauff, "Capacity fading in lithium/sulfur batteries: A linear four-state model," *J. Power Sources*, vol. 267, pp. 648–654, Dec. 2014, doi: 10.1016/j.jpowsour.2014.05.076.

[11] I. Baghdadi, O. Briat, P. Gyan, and J. M. Vinassa, "State of health assessment for lithium batteries based on voltage–time relaxation measure," *Electrochimica Acta*, vol. 194, pp. 461–472, Mar. 2016, doi: 10.1016/j.electacta.2016.02.109.

[12] R. Rao, S. Vrudhula, and D. N. Rakhmatov, "Battery modeling for energy-aware system design," *Computer*, vol. 36, no. 12, pp. 77–87, Dec. 2003, doi: 10.1109/mc.2003.1250886.

[13] C. Lin, H. Mu, R. Xiong, and J. Cao, "Multi-model probabilities based state fusion estimation method of lithium-ion battery for electric vehicles: State-of-energy," *Appl. Energy*, vol. 194, pp. 560–568, May 2017, doi: 10.1016/j.apenergy.2016.05.065.

[14] H. Verdejo, A. Awerkin, E. Saavedra, W. Kliemann, and L. Vargas, "Stochastic modeling to represent wind power generation and demand in electric power system based on real data," *Appl. Energy*, vol. 173, pp. 283–295, Jul. 2016, doi: 10.1016/j.apenergy.2016.04.004.

[15] K. Cai, Y. Liu, X. Lang, L. Li, Q. Zhang, T. Xu, and D. Chen, "Design of cobalt-based metal-organic frameworks like solid electrolyte interphase (SEI) film for chemically stable graphite anode of lithium-ion batteries," *Ionics*, vol. 26, no. 1, pp. 61–67, Jan. 2020, doi: 10.1007/s11581-019-03195-y.

[16] D. Goers, M. E. Spahr, A. Leone, W. Märkle, and P. Novák, "The influence of the local current density on the electrochemical exfoliation of graphite in lithium-ion battery negative electrodes," *Electrochim. Acta*, vol. 56, pp. 3799–3808, Apr. 2011, doi: 10.1016/j.electacta.2011.02.046.

[17] B. Saha and K. Goebel, "Battery data set," NASA Ames Prognostics Data Repository, NASA Ames Res. Center, Moffett Field, CA, USA, Tech. Rep., 2007. [Online]. Available: http://ti.arc.nasa.gov/project/prognostic-data-repository

[18] M. A. Mohamed and M. A. Deriche, "An approach for ECG feature extraction using daubechies 4 (DB4) wavelet," *Int. J. Comput. Appl.*, vol. 96, no. 12, pp. 36–41, Jun. 2014, doi: 10.5120/16850-6712.

[19] G. Dong, Z. Chen, J. Wei, and Q. Ling, "Battery health prognosis using Brownian motion modeling and particle filtering," *IEEE Trans. Ind. Electron.*, vol. 65, no. 11, pp. 8646–8655, Nov. 2018, doi: 10.1109/TIE.2018.2813964.

[20] Y.-J. He, J.-N. Shen, J.-F. Shen, and Z.-F. Ma, "State of health estimation of lithium-ion batteries: A multiscale Gaussian process regression modeling approach," *AIChE J.*, vol. 61, no. 5, pp. 1589–1600, May 2015, doi: 10.1002/aic.14760.

[21] D. Liu, Y. Luo, J. Liu, Y. Peng, L. Guo, and M. Pecht, "Lithium-ion battery remaining useful life estimation based on fusion nonlinear degradation AR model and RPF algorithm," *Neural Comput. Appl.*, vol. 25, nos. 3–4, pp. 557–572, Sep. 2014, doi: 10.1007/s00521-013-1520-x.
[22] Y. Choi, S. Ryu, K. Park, and H. Kim, "Machine learning-based lithium-ion battery capacity estimation exploiting multi-channel charging profiles," *IEEE Access*, vol. 7, pp. 75143–75152, 2019, doi: 10.1109/ACCESS.2019.2920932.

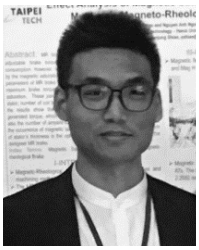

LAIFA TAO received the B.Sc. and Ph.D. degrees from the School of Reliability and Systems Engineering, Beihang University, in 2010 and 2014, respectively.

He is currently an Associate Professor with the School of Reliability and Systems Engineering, Beihang University. His research interests include fault diagnosis, prognostics, health state assessment, optimization and determination, and health management for electromechanical systems.

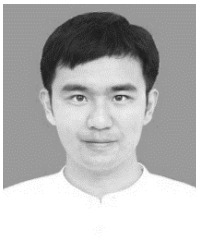

TONG ZHANG received the M.S. degree from the School of Mechatronical Engineering, Beijing Institute of Technology, in 2017. He is currently pursuing the Ph.D. degree with the School of Reliability and Systems Engineering, Beihang University.

His research interests include fault diagnosis, prognostics, health state assessment, knowledge-data fusion, and health management in the aerospace field.

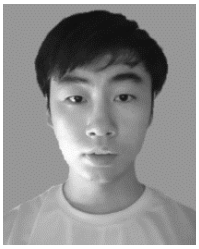

JIE HAO received the B.E. degree from the School of Reliability and Systems Engineering, Beihang University, in 2019, where he is currently pursuing the master's degree.

His research interests include fault diagnosis, prognostics, and health state assessment.

XIAOLIN WANG received the M.S. degree from Jilin University, in 2006. Since 2006, she has been with the Beijing Institute of Control and Electronic Technology, where she is currently a Senior Engineer. Her current research interests include data mining, decision making, performance evaluation, embedded software design, and algorithm design and optimization.

CHEN LU was born in 1974. He received the B.Sc. degree in electronics engineering and the Ph.D. degree in power engineering from the Dalian University of Technology, China, in 1996 and 2002, respectively.

From 2002 to 2007, he was a Postdoctoral Researcher with the Department of Automation, Tsinghua University, China, an Associate Professor with the Institute of Automation, Chinese Academy of Sciences, a Postdoctoral Research Fellow with the Department of Mechanical Engineering, ParisTech-ENSAM, France, and a Visiting Scholar with the Department of Industry Engineering, University of Wisconsin–Madison, USA, successively. Since 2007, he has been working with the School of Reliability and Systems Engineering, Beihang University, China. He is currently a Full Professor and an Executive Deputy Director of the State Key Laboratory for Reliability and Environmental Engineering, Beihang University. He is also the Team Leader of the National Science and Technology Innovation Team and a Distinguished Professor with the Key Laboratory of Aviation Technology for Fault Diagnosis and Health Management Research. He is the author of 100 academic articles and two books, and holds more than 30 patents. His current research interests include fault detection, diagnosis, and prognostics and system health management.

Dr. Lu is a Technical Member of the Professional Board Fault Diagnosis and Safety for Technical Process of the Chinese Association of Automation. He was a recipient of the Second-Class Prize of National Science and Technology Progress Award, in 2018, the First-Class Prize of National Defense Science and Technology Progress Award, in 2017 and 2015, the Second-Class Prize of National Defense Science and Technology Progress Award, in 2013, and the Elsevier Crossley Award for Distinguished Article and Conference Best Paper Awards. He has received many national and industrial research funds as a Principal Investigator, including the National Key Basic Research Program of China and the National Natural Science Foundation of China. He is also an Associate Editor or a Guest Editor for several international journals and serves as the Chair or the Co-Chair for several international conferences.

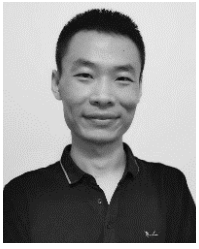

MINGLIANG SUO (Member, IEEE) received the B.S. degree from the School of Energy and Power Engineering, Beijing University of Aeronautics and Astronautics, China, in 2009, and the M.S. and Ph.D. degrees from the School of Astronautics, Harbin Institute of Technology, in 2013 and 2018, respectively. Since 2018, he has been with the School of Reliability and Systems Engineering, Beijing University of Aeronautics and Astronautics, where he is currently a Postdoctoral Fellow. He is also a member of the Science and Technology on Reliability and Environmental Engineering Laboratory. His current research interests include artificial intelligence, state-of-health assessment, decision-making, data mining, granular computing, prognostics and health management, and maintenance of aero-engine and aircraft.

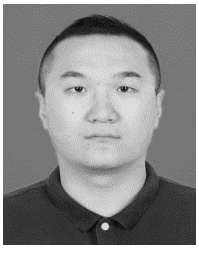

YU DING received the B.S. degree in electronic engineering, the M.S. degree in industrial engineering, and the Ph.D. degree in systems engineering from Beihang University, China, in 2013, 2016, and 2019, respectively. His research interests include intelligent fault diagnosis and prognostics of electromechanical systems, especially deep learning and deep reinforcement learning-based methods.